



**Vapor and Healing Treatment for $\text{CH}_3\text{NH}_3\text{PbI}_{3-x}\text{Cl}_x$ Films
Toward Large-Area Perovskite Solar cells**

Journal:	<i>Nanoscale</i>
Manuscript ID	NR-ART-12-2015-008658
Article Type:	Paper
Date Submitted by the Author:	05-Dec-2015
Complete List of Authors:	Gouda, Laxman; Bar Ilan University, BINA, Department of Chemistry Gottesman, Ronen; Bar Ilan University, Chemistry Tirosh, Shay; Bar-Ilan University, Department of Chemistry Haltzi, Eynav; Bar-Ilan University, Department of Chemistry Hu, Jiangang; Bar-Ilan University, Department of Chemistry Ginsburg, Adam; Bar-Ilan University, Department of Chemistry Keller, David; Bar-Ilan University, Department of Chemistry Bouhadana, Yaniv; Bar-Ilan University, Department of Chemistry Zaban, Arie; Bar-Ilan University, Department of Chemistry



Nanoscale

ARTICLE

Received 00th January 20xx,
Accepted 00th January 20xx

DOI: 10.1039/x0xx00000x

www.rsc.org/

Vapor and Healing Treatment for $\text{CH}_3\text{NH}_3\text{PbI}_{3-x}\text{Cl}_x$ Films toward Large-Area Perovskite Solar cells

Laxman Gouda,[†] Ronen Gottesman,[†] Shay Tirosh, Eynav Haltzi, Jiengang Hu, Adam Ginsburg, David A. Keller, Yaniv Bouhadana and Arie Zaban*

Hybrid methyl-ammonium lead trihalide perovskites are promising low-cost materials for use in solar cells and other optoelectronic applications. With a certified photovoltaic conversion efficiency record of 20.1%, scale-up for commercial purposes is already underway. However, preparation of large-area perovskite films remains a challenge, and films of perovskites on large electrodes suffer from non-uniform performance. Thus, production and characterization of the lateral uniformity of large-area films is a crucial step towards scale-up of devices. In this paper, we present a reproducible method for improving the lateral uniformity and performance of large-area perovskite solar cells (32 cm²). The method is based on methyl-ammonium iodide (MAI) vapor treatment as a new step in the sequential deposition of perovskite films. Following the MAI vapor treatment, we used high throughput techniques to map the photovoltaic performance throughout the large-area device. The lateral uniformity and performance of all photovoltaic parameters (V_{oc} , J_{sc} , Fill Factor, Photo-conversion efficiency) increased, with an overall improved photo-conversion efficiency of ~ 100% following a vapor treatment at 140 °C. Based on XRD and photoluminescence measurements, We propose that the MAI treatment promotes a "healing effect" to the perovskite film which increases the lateral uniformity across the large-area solar cell. Thus, the straightforward MAI vapor treatment is highly beneficial for large scale commercialization of perovskite solar cells, regardless of the specific deposition method.

Introduction

Photovoltaic devices based on solution processed methyl-ammonium (MA) lead trihalide perovskite absorbers ($\text{CH}_3\text{NH}_3\text{PbX}_3$, or MAPbX_3 where X= Br, Cl, I) have been recognized as promising candidates for solid-state junction devices, with certified efficiencies of up to 20.1%.¹ The superior optoelectronic properties and inexpensive deposition methods renders perovskites highly attractive and adaptable materials. Since 2009, perovskite solar cells (PSCs) have rapidly evolved from being used in dye sensitized solar cell configuration,² to implementation into three other device architectures,^{1,4,5} all yielding remarkable efficiencies of over 15%. In addition, hybrid perovskite have been implemented in other photovoltaic technologies, sensors and light emitting

Department of Chemistry, Center for Nanotechnology & Advanced Materials, Bar Ilan University, Ramat Gan 52900, Israel. Email: zabana@mail.biu.ac.il

[†] L.G and R.G contributed equally to this work.

Electronic Supplementary Information (ESI) available. See DOI: 10.1039/x0xx00000x

devices.^{6,7} The most commonly used perovskites in PSCs are the MAPbI₃ or the mixed halide MAPbI_{3-x}Cl_x which possess a bandgap of ~1.55 eV that enables absorbance of the full visible-light range.⁸⁻¹⁰ As PSCs have such high efficiencies, scale-up for commercial purposes is the subject of intense research.¹¹ However, preparation of large-area perovskite films is still challenging and devices with larger electrodes suffer from low performance lateral uniformity.¹²

To date, the most common used deposition technique for MAPbX₃ perovskite films on different small-area substrates is the convenient and inexpensive sequential (two-step) deposition method.⁴ First, a film of PbX₂ is deposited on a substrate by spin coating. Next, the annealed film is dipped into a methyl-ammonium halide (MAX) solution for a short period of time (tens of seconds to a few minutes). This promotes the intercalation of MAX into the PbX₂ lattice to form MAPbX₃ and is followed by a final annealing step. Despite being a straightforward deposition technique that is used in the fabrication of efficient PSCs, the two-step method is challenged by two major shortcomings: i) prolonged dipping in the MAX solution results in peeling of the film from the substrate.¹³ As a result, dipping times are kept to a minimum, leaving unconverted PbX₂ phase in the film, which is not detrimental to the efficiency and stability solar cells but should be avoided for optimal performances.¹⁴ ii) Deposition on large-area substrates is prone to result in low quality perovskite films. Also, regardless of the specific deposition method, when depositing on large-area substrates, forming distinct perovskite islands with voids between them instead of a uniform perovskite film is common under non-optimized deposition conditions.^{15,16} This lack of lateral uniformity decreases the quality of the optoelectronic properties, makes effective reproducibility impossible and is a major concern in scale-up of PSCs. To overcome the lack of lateral uniformity in up-scaling, either special care must be taken to "heal" the large-area substrates, or new and probably more expensive deposition methods must be employed.

Furthermore, characterizing and mapping the physical, structural and optical properties of large-area films is a crucial step towards any scale-up of devices. There are many methods of characterization, either assessing the entire film in a single measurement or *in situ* characterization by spectroscopy. In some cases, the film is divided into small-area segments that are measured separately and maps of the different physical parameters throughout the large-area device are created. The latter is highly advantageous and has many potential applications. In order to probe many segments on one film, high-throughput scanning systems need to be utilized.¹⁷⁻¹⁹ The use of high throughput analysis of solar cell has many advantages over the single measurements. The number of separate back contacts can be easily controlled on a large-area substrate by the use of different evaporation mask sizes. The use of multiple small-area solar cells on a single large-area solar cell increases the number of characterization techniques that could be performed.²⁰ For example, a critical advantage of such mapping is that we bypass the issue of Fill Factor (FF) in large-area solar cells, where high currents bring a significant

drop in the FF. The mapping gives us accurate localized information on what is the actual FF in a certain segment of the large-area solar cell.

In this study, we introduce a new method which is suitable for scale-up of large-area perovskite solar cells. A MAI vapor treatment was added as a post-deposition step to the standard two-step perovskite deposition method on large-area substrates. The vapor treatment was performed in the temperature range of 100-140 °C in comparison to the reference that did not undergo vapor treatment. For this we used large-area fluorine doped tin oxide (FTO) glasses (71×71 mm²) onto which we deposited all layers of a full PSC; compact and mesoporous TiO₂ layers, MAPbI_{3-x}Cl_x and spiro-OMeTAD as the hole transport material. The deposition of the MAPbI_{3-x}Cl_x was performed using the sequential deposition technique. The benefits of the MAI vapor treatment are: a) unconverted PbI₂ can be converted to perovskite without the risk of peeling off that occurs during prolonged exposure to MAI solution, b) this post-deposition vapor treatment can be easily controlled and is applicable to all hybrid perovskites deposition methods, c) easy to perform on large-area films, d) as will be demonstrated in this study, the vapor treatment has a healing effect on the perovskite after the standard deposition method.

In order to assess lateral uniformity of the large-area film, we deposited circular silver contacts, creating a "library" of 121 individual small area PSCs (single contact area = 0.026 cm²), as seen in Figure 1 (Note: since a small area brings concerns of overestimation we calibrated our systems with and without a shadow mask and we found that there is no reasonable error). The periphery area close to the edges of the large substrate was not measured, due to concerns that the contacts' soldering might affect. This configuration enabled us to perform 121 separate iV measurements across the large PSC area, to generate iV maps of photovoltaic parameters. The iV maps of the reference library showed low lateral uniformity in the parameters and the highest efficiency was 8%, which is appreciable for large-area films prepared by the standard sequential two-step technique but represents a significant penalty large-area. In contrast, the PSCs treated with MAI vapor displayed an increase in lateral uniformity of the parameters and efficiencies close to 16%. The deposition of high quality and uniform perovskite films with uniform performance following mapping of the entire working area demonstrates a potential technique for the scale-up of perovskite solar cells.

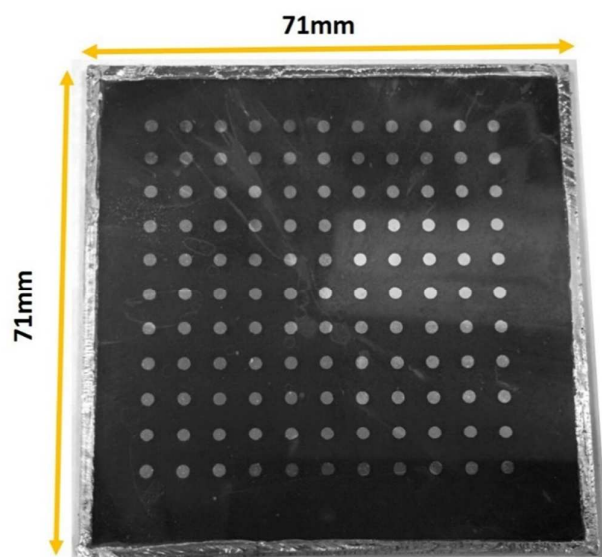


Figure 1. Photograph of a library with 121 separate PSCs (each cell area is 0.026 cm²) on a single large-area (71×71 mm²) substrate.

Experimental details and device fabrication

The materials and chemicals used in this study for the fabrication of devices were purchased as follows: FTO TEC-15 (Hardford Glass), titanium-tetraisopropoxide (Sigma-Aldrich), TiO₂ paste (18NRT, Dyesol), PbI₂, PbCl₂ (Sigma-Aldrich), DMSO (Fisher Scientific), 2-propanol (J.T.Baker), spiro-OMeTAD (Merck), chlorobenzene (Alfa Aesar), acetonitrile (J.T.Baker), bis(trifluoromethylsulfonyl)imide lithium salt (Sigma Aldrich), and 4-*tert*-butylpyridine, (Sigma-Aldrich).

TEC-15 fluorine-doped tin oxide coated glass (71×71 mm²) was used as the substrate for the fabrication of devices. Each substrate was thoroughly cleaned with detergent, water and ethanol before treatment with argon plasma for 4 minutes. The compact TiO₂ blocking layer was deposited by a spray pyrolysis system.¹⁷ A precursor solution of 0.1M titanium-tetraisopropoxide and acetyl acetone (1:1 ratio) in ethanol was sprayed on the pre-heated (450 °C) substrates. A 250-300 nm thick mesoporous scaffold TiO₂ layer was produced by spinning a TiO₂ paste (diluted with ethanol at 1:10 ratio) at 5000 rpm for 30 seconds. The film was then annealed at 550 °C for 90 minutes.

The mixed halide lead solution was prepared using a 1M:0.06M ratio of PbI₂:PbCl₂ dissolved in DMSO and then stirred at 80 °C overnight. The MAI solution was prepared (32 mg/mL in 2-propanol) at 60 °C. The synthesis of the MAI powder is described elsewhere.²¹ The mixed halide lead solution was spin coated at 4000 rpm for 60 seconds onto the mesoporous TiO₂ electrode and the film was subsequently annealed at 100 °C for 1 hour. The halide lead films were dipped in a 60 °C solution of MAI for 2 minutes and then washed with 2-propanol. 50 μL of toluene was spun at 4000 rpm onto the perovskite film. The perovskite film was held upside down in a MAI vapor environment for 1 hour in a Pyrex glass box containing 200 mg of MAI powder heated in the

range of 100 to 140 °C. This was followed by annealing at 100 °C for 1.5 hour.

The hole transport material (HTM), Spiro-OMeTAD, was dissolved in chlorobenzene (72 mg/mL) with the addition of 34 μL (540 mg/mL in acetonitrile), bis-(trifluoromethylsulfonyl)-imide lithium salt (LiTFSI) and 58 μL (80 mM) 4-*tert*-butylpyridine (TBP). The HTM solution was spin coated onto the perovskite films at 4000 rpm for 30 seconds. The substrates were kept in a dry box (air environment) overnight under dark conditions to dope the HTM with oxygen. A grid of 11×11 cells with 100 nm silver back contacts were thermally evaporated with an area of ~0.026 cm².

iV scans were performed using a home built automated scanner. Absorption measurements were recorded using a CARY UV-Vis-NIR spectrophotometer and the fluorescence measurements were performed on a CARY Eclipse Fluorescence Spectrophotometer. X-ray diffraction (XRD) measurements were performed on a Bruker D8 advanced X-ray diffractometer.

Results and discussion

The two-step synthesis of perovskite was modified by adding an additional step of exposing the perovskite films to MAI vapors for a duration of 1 hour. After the vapor treatment, the films were annealed followed by hole transporting material deposition. Figure 2 illustrates the full synthesis procedure for the PSCs. In step 1, the PbI_{2-x}Cl_x was deposited on mesoporous TiO₂ followed by heating. In a step 2 the mixed halide lead film was dipped into hot MAI solution, where MAI intercalated into the PbI₂ lattice to form MAPbI_{3-x}Cl_x. In Step 3 toluene was spin coated onto the perovskite. Finally, the perovskite was exposed to MAI vapor at 100, 120 and 140 °C, followed by annealing.

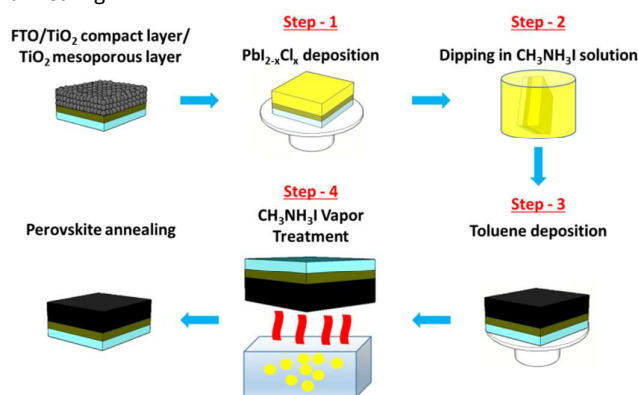


Figure 2. Schematic diagram of the synthesis procedure of PSCs. In addition to the standard two-step deposition method, we added a toluene treatment (step 3) followed by a MAI vapor treatment (step 4).

The performed iV mapping and photovoltaic parameters of four libraries (descending curve) are shown in Figure 3. The four libraries are; reference library (no MAI treatment) and libraries exposed to MAI vapors at 100, 120 and 140 °C. The reference library shows poor and inhomogeneity in device

performance and libraries with MAI vapor treatment, shows improvement in the lateral uniformity of performance which increases with the vapor treatment temperature. Heating at lower temperatures was not beneficial while higher temperatures resulted in damage to the libraries. At temperatures lower than 100 °C the MAI vapor pressure is not high enough to improve the device performance within a time scale of 1 hour. The V_{oc} , J_{sc} , FF and photo-conversion efficiency (PCE) across the reference library were not uniform. However, with increasing MAI vapor treatment temperature, the lateral uniformity of all parameters increased. Under optimized procedures an efficiency of up to 16% in the MAI@140 °C library was attained.

The descending iV curve of the best PSC of each library is presented in Figure 4, while Table 1 summarizes the photovoltaic parameters. The improvement in photovoltaic performance and minimization of the hysteresis after MAI

vapor treatment is evident. The J_{sc} , V_{oc} , FF and PCE increased with vapor treatment temperature compared to the reference solar cells. The champion cell which is vapor treated at 140 °C shows 20.2 mA current, 1.1 V voltage and 15.6 % efficiency.

The statistics of all 121 PSCs from the four different libraries are shown Figure 5. The increase of all parameters following the vapor treatments goes together with better lateral uniformity in terms of standard deviation and distribution. By performing the MAI vapor treatment, a transition is made from a low performance large-area PSC where a big contact area would result in electrical shortcuts to a PSC that can operate well with a large-area back contact. This increase can be attributed to the penetration of MAI into the perovskite layer, which improves its quality and uniformity. In order to better understand how the MAI vapor treatment affected the PSCs, we studied the absorption, photoluminescence and crystallographic structure of all four libraries.

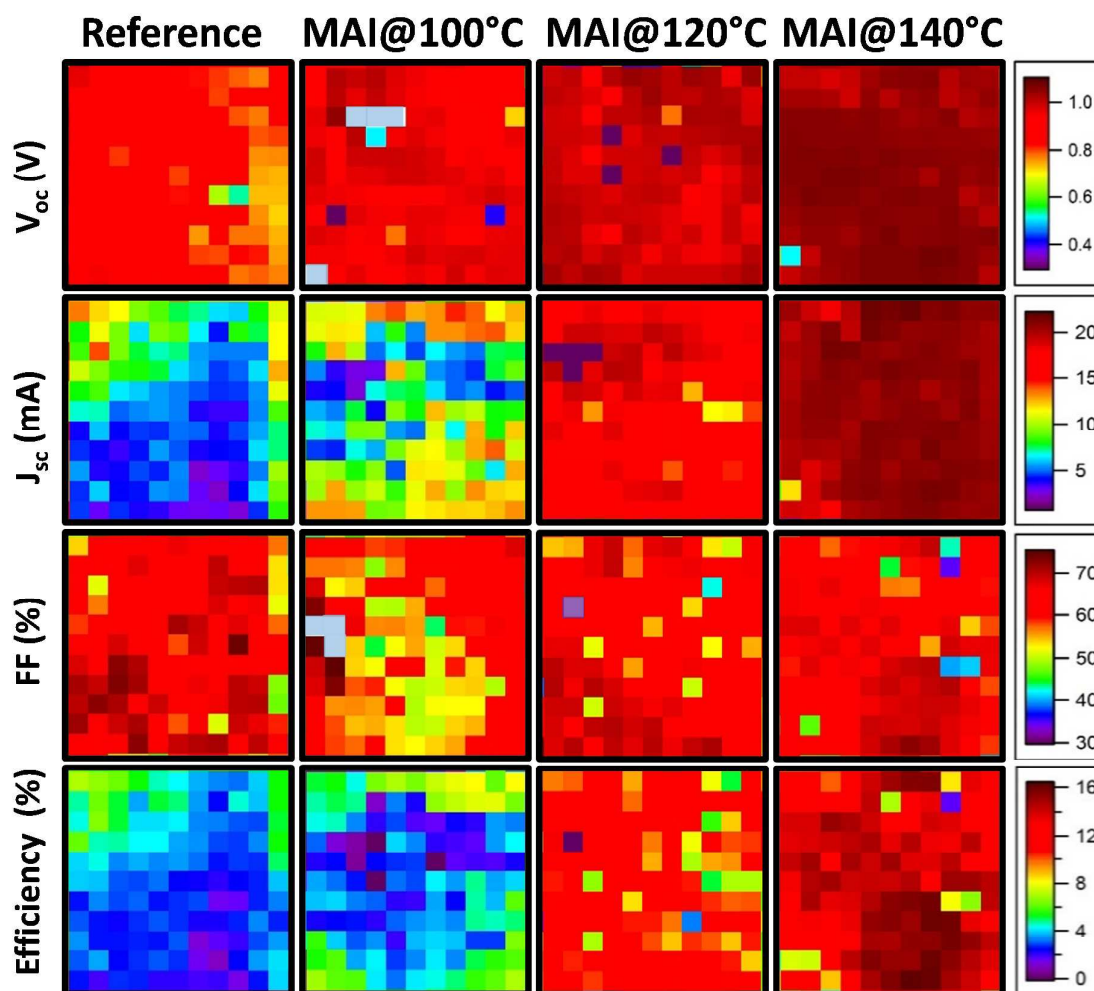


Figure 3. The iV maps of the photovoltaic parameters (descending curves only) of all four libraries: reference library (no MAI treatment) and libraries exposed to MAI vapors at 100, 120 and 140 °C.

Nanoscale

ARTICLE

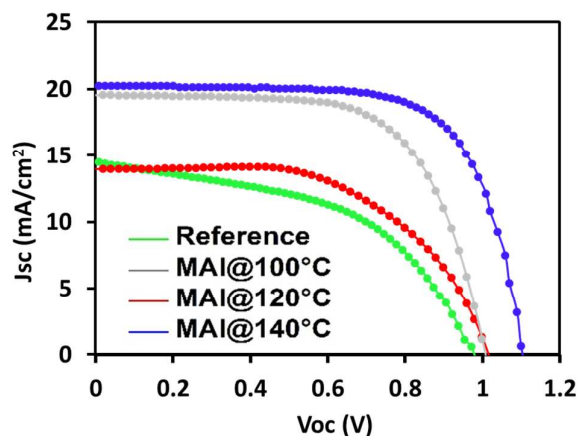


Figure 4. The descending IV curve of the best PSC from each of the four libraries.

Table 1. A summary of the photovoltaic parameters of the best PSC from each library taken from the iV curves in Figure 4.

	Ascending scan				Descending scan			
	J_{sc} (mA/cm^2)	V_{oc} (V)	FF (%)	Efficiency (%)	J_{sc} (mA/cm^2)	V_{oc} (V)	FF (%)	Efficiency (%)
Reference	14.5	0.98	50	7.0	15.5	1.00	57	8.9
MAI@100 °C	14.4	1.02	53	7.8	14.6	1.02	58	8.2
MAI@120 °C	19.2	1.00	58	11	19.2	1.02	65	12.5
MAI@140 °C	20.2	1.1	69	15.5	20.2	1.1	70	15.6

X-Ray Diffraction (XRD) measurements of perovskite films deposited on reference and vapor treated electrodes composed of FTO/compact TiO_2 /mesoporous TiO_2 are presented in Figure 6. The exposure of the perovskite film to MAI vapors for extended periods before annealing under ambient dry air conditions was shown to induce complete conversion of PbI_2 film into MAPbI_3 . The main PbI_2 peak (labeled L1 in Fig 6) at $12.3^\circ 2\theta$, significantly decreased in intensity in the film following vapor treatment. As discussed above, full conversion of the PbX_2 into MAPbX_3 perovskite in a standard sequential deposition is non-trivial with increasing difficulty as the film thickness increases. Here, the vapor treatment allowed a longer reaction time at high temperatures, enabling the PbI_2 to fully convert to perovskite without degradation.

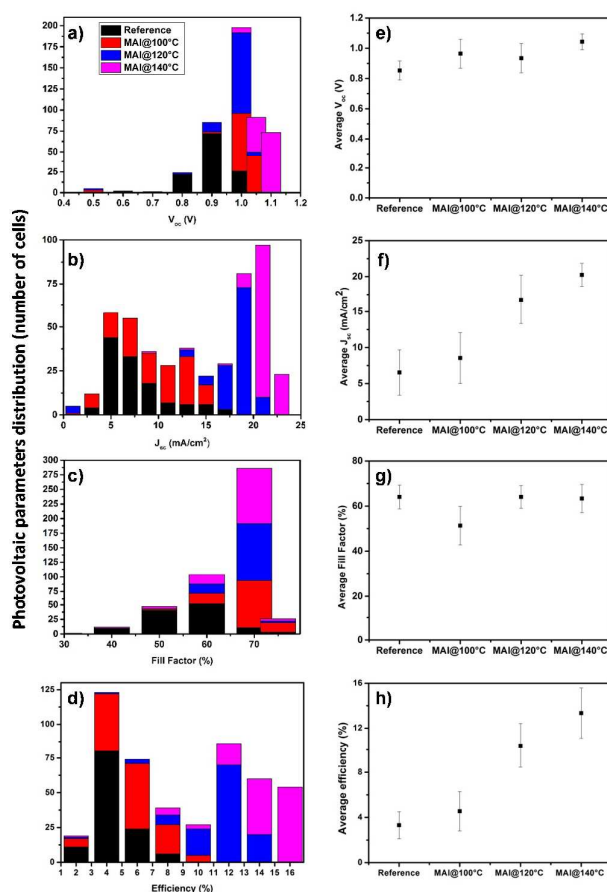


Figure 5. a-d) Photovoltaic parameters statistical distribution taken from 484 PSCs in all four libraries, presented in a column stack manner. e-h) The average values of the i-V parameters of each library, with the standard deviation.

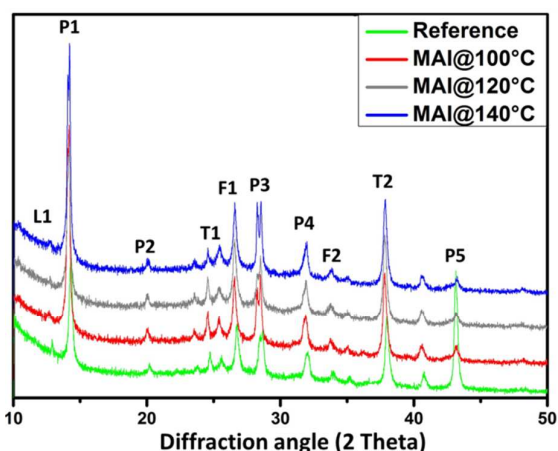


Figure 6. XRD spectra of $\text{MAPb}_{1-x}\text{Cl}_x$ deposited on FTO/compact TiO_2 /mesoporous TiO_2 substrates of all four libraries. P, L, T and F correspond to the perovskite, PbI_2 , TiO_2 and FTO peaks respectively.

Sharp and well defined perovskite peaks ("P" in Figure 6) were observed at 13.9° , 14.2° , 19.97° , 28.1° , 28.6° , 32.13° , 42.93° , corresponding to the (002), (110), (112), (004), (220), (130) and (134) planes, respectively. A few peaks of Anatase TiO_2 ("T") 25.34° (011), 38.57° (112) and FTO ("F") 26.48° (110), 33.7° (020) planes were also assigned in XRD spectra (Figure 6).^{22,23}

Our analysis utilized subtle changes in the XRD patterns of the different samples to describe vapor treatment induced crystallographic modification. The analysis was performed by considering three possible perovskite crystal structures; cubic (C) - $\text{Pm}3\text{m}$, pseudo-cubic (PC) – $\text{P}4\text{mm}$ and tetragonal (TG) – $\text{I}4/\text{mcm}$ symmetry groups.²⁴ For simplicity, the XRD analysis was conducted under the assumption that no severe strains and no orientations exist in the perovskite films.

The grain size and wt/wt% were analyzed and are presented in Figure S1. A dependency on the grains size and wt/wt% on the MAI vapor treatment temperature was observed. The grain size of the tetragonal and pseudo-cubic phases grew at the expense of the cubic phase with increasing MAI vapor treatment temperature.^{25,26} The wt/wt% showed that the percentage of tetragonal and pseudo-cubic structures increased with the vapor treatment temperature and that the cubic phase disappeared at the high temperatures due to thermodynamic stability process. During MAI vapor treatment, the grain size increased due to a coarsening effect which minimized the grain boundaries. This might decrease voids and defects in the film, promoting a "healing effect" to the perovskite. As a result, the performance and lateral uniformity across the large PSC area were considerably enhanced.

In order to examine the effect of MAI vapors on the perovskite absorbance, we performed UV-Vis measurements of perovskite films deposited on FTO/compact TiO_2 /mesoporous TiO_2 electrodes (Figure 7). There was a notable increase in the absorbance after MAI treatment, probably due to the increased PbI_2 conversion to perovskite at higher vapor temperatures, which correlated with the XRD data.

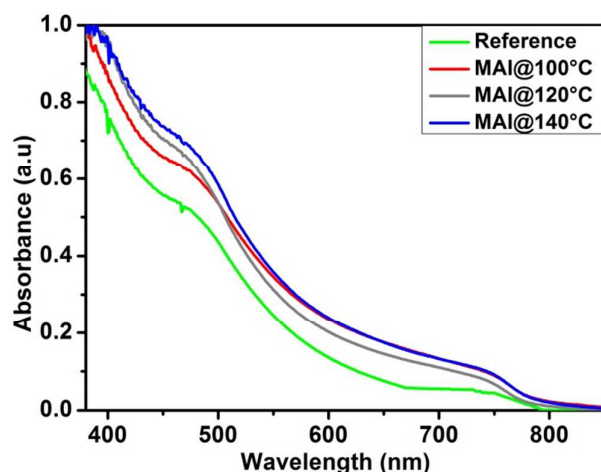


Figure 7. The absorbance spectra of perovskite films deposited on FTO/compact TiO_2 /mesoporous TiO_2 substrates for all four libraries. The absorbance increases with the MAI treatment temperature in comparison to the untreated sample.

In addition, photoluminescence (PL) measurements were performed to examine changes in radiative recombination of photo-carriers in the different perovskite libraries. The measured substrates composition was $\text{MAPb}_{1-x}\text{Cl}_x$ /mesoporous TiO_2 /compact TiO_2 /FTO glass and the emission peak was at 770 nm (Figure 8). In all samples, there was no shift in the emission peak. However, a decrease in the intensity with increasing MAI vapor temperature was noticed. This suggests a better charge transfer to the TiO_2 in the MAI treated substrates, which is in agreement with the higher efficiencies achieved as the MAI vapor temperatures increased. This interpretation was confirmed by PL measurements of identical electrodes that were deposited on glass rather than on TiO_2 showing similar PL intensity for the reference electrode and the three MAI treated electrodes.

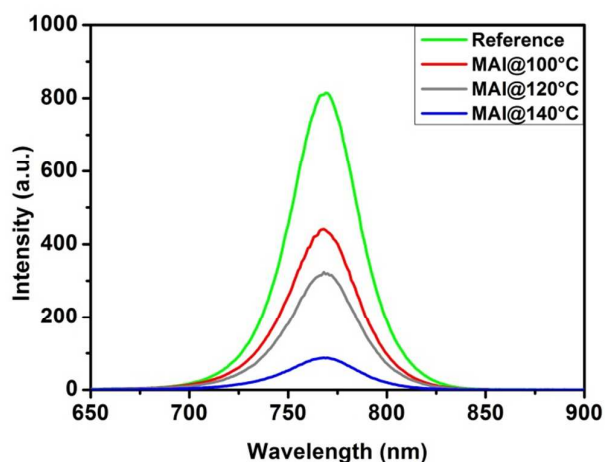


Figure 8. The fluorescence spectra of perovskite films deposited on FTO/compact TiO_2 /mesoporous TiO_2 substrates for all four libraries. The peak intensity of the MAI treated samples decreases with MAI treatment temperature in comparison to the reference.

Conclusions

In this study, we demonstrated a fabrication method of large-area perovskite solar cells with high lateral uniformity and performance. This was achieved by the introduction of an additional MAI vapor treatment step to the standard sequential deposition method of $\text{MAPbI}_{3-x}\text{Cl}_x$ perovskites. The MAI vapor treatment was performed in the temperature range of 100–140°C. Using this approach we fabricated mesoscopic solar cells on large-area substrates and assessed their photovoltaic performance by dividing them into 121 smaller PSCs. The gathered photovoltaic data from all 121 PSCs enabled us to map the lateral uniformity and performance of the large-area PSC. The IV mapping of four different large-area substrates showed an increase in efficiency throughout their large-area with improved lateral uniformity of all photovoltaic parameters after the MAI vapor treatments, in comparison to the reference. Overall, the photo-conversion efficiency improved by ~ 100% following a vapor treatment at 140 °C. XRD studies showed disappearance of the PbI_2 phase as the temperature of the MAI vapors increased which was also correlated with an increase in the optical density of the films. We propose that the MAI treatment promotes a "healing effect" to the perovskite which increases the lateral uniformity across the large-area solar cell. Regardless of the perovskite specific deposition method, the use of MAI vapors is a straightforward and effective way to achieve reproducible and efficient perovskite devices on large-area solar cells.

Acknowledgements

We thank the Israel Strategic Alternative Energy Foundation (I-SAEF) and the 'Tashtiyot' Program of the Israeli Ministry of Science & Technology for funding R.G and L.G from the European Union Seventh Framework Program Destiny Project, under grant 316494. Special thanks to Mr. Eli Rosh Hodesh for assistance in performing the high throughput characterization of the devices.

Notes and references

- 1 W. S. Yang, J. H. Noa, N. J. Jeon, Y. C. Kim, S. Ryu, J. Seo, S. Il. Seok, *Science*, 2015, **348**, 1234-1237.
- 2 A. Kojima, K. Teshima, Y. Shirai, T. Miyasaka, *J. Am. Chem. Soc.* 2009, **131**, 6050-6051.
- 3 M.M. Lee, J. Teuscher, T. Miyasaka, T. N. Murakami, H. J. Snaith, *Science*, 2012, **338**, 643-647.
- 4 J. Burschka, N. Pellet, S. J. Moon, R. H. Baker, P. Gao, M. K. Nazeeruddin, M. Gratzel, *Nature*, 2013, **499**, 316-319
- 5 M. Liu, M. B. Johnston, H. J. Snaith, *Nature*, 2013, **501**, 395-398.
- 6 F. Deschler, M. Price, S. Pathak, L. Klintberg, D. D. Jarausch, R. Higler, S. Huttner, T. Leijtens, S. D. Stranks, H. J. Snaith, M. Atature, R. T. Phillips, R. H. Friend, *J. Phys. Chem. Lett.* 2014, **5**, 1421-1426.

- 7 B. R. Sutherland, A. K. Johnston, H. Ip. Alexander, J. Xu, V. Adinolfi, P. Kanjanaboos, E. H. Sargent, *ACS Photonics*, 2015, **2**, 1117-1123.
- 8 V. D'Innocenzo, A. R. S. Kandada, M. De'Bastiani, M. Gandini, A. Petrozza, *J. Am. Chem. Soc.* 2014, **136**, 17730-17733.
- 9 J. M. Frost, K. T. Butler, F. Brivio, C. H. Hendon, M. Van Schilfgaarde, A. Walsh, *Nano Lett.* 2014, **14**, 2584-2590.
- 10 Z. Zhu, J. Ma, Z. Wang, C. Mu, Z. Fan, L. Du, Y. Bai, L. Fan, H. Yan, D. L. Phillips, S. Yang, *J. Am. Chem. Soc.* 2014, **136**, 3760-3763.
- 11 K. Hwang, Y. S. Jung, Y. J. Heo, F. H. Scholes, S. E. Watkins, J. Subbiah, D. J. Jones, D. Y. Kim, D. Vak, *Adv. Mater.* 2015, **27**, 1241-1247.
- 12 F. Matteocci, S. Razza, F. Di Giacomo, S. Casaluci, G. Mincuzzi, T. M. Brown, A. D'Epifanio, S. Licocciab, A. Di Carlo, *Phys. Chem. Chem. Phys.* 2014, **16**, 3918-3923.
- 13 Y. Wu, A. Islam, X. Yang, C. Qin, J. Liu, K. Zhang, W. Peng, L. Han, *Energy Environ. Sci.* 2014, **7**, 2934-2938.
- 14 Y. Zhao, K. Zhu, *J. Phys. Chem. Lett.* 2014, **5**, 4175-4186.
- 15 G. E. Eperon, V. M. Burlakov, P. Docampo, A. Goriely, H. J. Snaith, *Adv. Funct. Mater.* 2014, **24**, 151-157.
- 16 A. T. Barrows, A. J. Pearson, C. K. Kwak, A. F. Dunbar, A. R. Buckleya, D. G. Lidzey, *Energy Environ. Sci.* 2014, **7**, 2944-2950.
- 17 A. Y. Anderson, Y. Bouhadana, H. N. Barad, B. Kupfer, E. Rosh-Hodesh, H. Aviv, Y. R. Tischler, S. Ruhle, A. Zaban, *ACS Comb. Sci.* 2014, **16**, 53-65.
- 18 S. Ruhle, A. Y. Anderson, H. N. Barad, B. Kupfer, Y. Bouhadana, E. Rosh-Hodesh, A. Zaban, *J. Phys. Chem. Lett.* 2012, **3**, 3755-3764.
- 19 K. Shimanovich, Y. Bouhadana, D. A. Keller, S. Ruhle, A. Y. Anderson, A. Zaban, *Rev. Sci. Instrum.* 2014, **85**, 55-103.
- 20 S. Ruhle, H. N. Barad, Y. Bouhadana, D. A. Keller, A. Ginsburg, K. Shimanovich, K. Majhi, R. Lovrincic, A. Y. Anderson, A. Zaban, *Phys. Chem. Chem. Phys.* 2014, **16**, 7066-7073.
- 21 R. Gottesman, E. Haltzi, L. Gouda, S. Tirosh, Y. Bouhadana, A. Zaban, *J. Phys. Chem. Lett.* 2014, **5**, 2662-2669.
- 22 T. Baikie, Y. Fang, J. M. Kadro, M. Schreyer, F. Wei, G. S. Mhaisalkar, M. Graetzel, T. J. White, *J. Mater. Chem. A*, 2013, **1**, 5628-5641.
- 23 M. Horn, C. Schwerdtfeger, *Switzerland Zeitschrift fur Kristallographie*. 1972, **136**, 273-281.
- 24 S. Grazulis, C. Daskevi, A. Merkys, D. Chateigner, L. Lutterotti, M. Quiros, N. R. Serebryanaya, P. Moeck, A. Downs, *Nucleic Acids Research* 2012, **40**, D420-D427.
- 25 S. Grazulis, D. Chateigner, R. T. Downs, A. T. Yokochi, M. Quiros, L. Lutterotti, E. Manakova, J. Butkus, P. Moeck, A. Le Bail, *J. Appl. Cryst.* 2009, **42**, 726-729.
- 26 R. T. Downs, M. Hall-Wallace, *American Mineralogist*. 2003, **88**, 247-250.